ARMA 22–0831

Computational Modeling of creep behavior in shales induced by fluid-rock interaction.

Prakash, R.
Texas A&M University, College Station, Texas, USA
Abedi, S.
Texas A&M University, College Station, Texas, USA

This paper was prepared for presentation at the 56th US Rock Mechanics/Geomechanics Symposium held in Santa Fe, New Mexico, USA, 26-29 June 2022. This paper was selected for presentation at the symposium by an ARMA Technical Program Committee based on a technical and critical review of the paper by a minimum of two technical reviewers. The material, as presented, does not necessarily reflect any position of ARMA, its officers, or members. Electronic reproduction, distribution, or storage of any part of this paper for commercial purposes without the written consent of ARMA is prohibited. Permission to reproduce in print is restricted to an abstract of not more than 200 words; illustrations may not be copied. The abstract must contain conspicuous acknowledgement of where and by whom the paper was presented.

ABSTRACT: The chemo-mechanical loading of rocks causes the dissolution and precipitation of multiple phases in the rock. This dissolution and precipitation of load-bearing mineral phases lead to the stress redistribution in neighboring phases, which in turn results in deformational changes of the sample composite. The aim of this study is to investigate the link between microstructural evolution and creep behavior of shale rocks subjected to chemo-mechanical loading through modeling time-dependent deformation induced by the dissolution-precipitation process. The model couples the microstructural evolution of the shale rocks with the stress/strain fields inside the material as a function of time. The modeling effort is supplemented with an experimental study where shale rocks were exposed to CO2-rich brine under high temperature and pressure conditions. 3D snapshots of the sample microstructure were generated using segmented micro-CT images of the shale sample. The time-evolving microstructures were then integrated with the Finite element-based mechanical model to simulate the creep induced by dissolution and precipitation processes independent of the intrinsic viscoelasticity/viscoplasticity of the mineral phases. After computation of the time-dependent viscoelastic properties of the shale composite, the combined microstructure model and finite element model were utilized to predict the time-dependent stress and strain fields in different zones of reacted shale.

1. INTRODUCTION

Determination of viscous behavior of shale rocks is key in wide range of applications such as stability of reservoirs, stability of geo-structures subjected to environmental forcing, underground storage of hazardous materials and hydraulic fracturing. Short- term creep strains in hydraulic fracturing can change stress fields and in turn can impact the hydraulic fracturing procedures(H. Sone & Zoback, 2010; Hiroki Sone & Zoback, 2013). While long-term creep strains can hamper the reservoir performance due to the reduction in permeability of the reservoir by closing of fractures and fissures(Du, Hu, Meegoda, & Zhang, 2018; Rybacki, Meier, & Dresen, 2016; Sharma, Prakash, & Abedi, 2019; Hiroki Sone & Zoback, 2014). Owing to these significance of creep strain, it is important to understand the viscoelastic/viscoplastic behavior of shales.

Many studies have been conducted to study the mechanism behind creep deformations of materials such as cement and quartz. It has been demonstrated that change in microstructure due to time dependent dissolution processes plays an important role in viscoelatic/viscoplastic deformations of the material. Therefore, microstructure evolution of shale rocks due to surface dissolution and precipitation processes can result in creep/relaxation deformations in the vicinity of the exposed surfaces. To study this creep deformation, a computational model scheme is implemented, which uses time evolving microstructure as input and uses finite element method to calculate the strain and stress field inside the material at every time step.

This study aims at utilizing nano-indentation data and micro-CT images of an Eagle Ford sample to calculate creep strains using finite element based mechanical model. 3D snapshots generated by Micro-CT imaging provides us with microstructure model of the shale sample. Nano-indentation gives us the spatial change in mechanical properties due to the dissolution and precipitation processes as a result of chemo-mechanical loading of the sample. Evolution of viscoelastic properties of the sample is estimated by coupling the microstructural evolution with the stress/strain fields inside the material as a function of time.

2. COMPUTATIONAL MODEL

This work is an implementation of a computational model which computes homogenized elastic properties of composite material and hence calculates the creep deformations in the composite (Garboczi, 1998; Haecker et al., 2005; Li, Rahman, & Grasley, 2016). First time evolving microstructures are generated at different time steps. These microstructures are three dimensional volumes of the composite material discretized as a cubical voxel and are generated for every time step of the reaction. Each of these voxels is considered to be a single element with eight nodes, each node attached to the vertex of the voxel. Each element is considered to be a homogeneous material and any change in microstructure at different times will be at elemental or voxel scale. At each time step, the change in the microstructure is a result of the phase alteration at any voxel or the change in mechanical properties of a particular phase without a phase alteration at that voxel.

The microstructure model is then integrated with a finite element based mechanical model. Finite element model is then utilized to compute the stress and strain fields at each time step, under strain controlled boundary conditions. These volume averaged stress and strain fields are then used to calculate the time evolving creep and mechanical properties of the composite.

2.1. Finite element calculation

The finite element calculation done here utilizes a previously built homogenization model to predict the elastic moduli of composites using 3D digital images (Garboczi, 1998). The input for the calculations are the 3D microstructures at different time steps. For a given microstructure at a certain time, subject to boundary conditions, the elastic displacement distribution should be such that the total energy stored is minimum. For this analysis each voxel/element is considered to be behaving as purely linearly elastic material. So at any time step, when the composite is subjected to infinitesimal strains, the total elastic energy stored in one voxel/element is given by the equation

$$En = \frac{1}{2}\int_0^1\int_0^1\int_0^1 \varepsilon_{pq} C_{pqrs} \varepsilon_{rs} dxdydz \tag{1}$$

where *En* is the total stored elastic energy, ε_{pq} and C_{pqrs} are the infinitesimal strain tensor and the elastic moduli in full tensorial form, p, q, r, s =1, 2 or 3, and the integral is over volume of a single voxel. Equation 1 can be represented in the form of displacement components by the following equation.

$$En = \frac{1}{2} u_{rp}^T D_{rp,sq} u_{sq} \tag{2}$$

where $D_{rp,sq}$ is the stiffness matrix and u_{rp} is the p^{th} component of displacement at the r^{th} node.

When an elastic material undergoing dissolution process is exposed to external load, then the whole composite and every element/ voxel of the body undergoes deformation form its initial, reference configuration to the current configuration. When the loading is removed, the composite will not return to its reference configuration but will go to the composite natural configuration. It has been seen that evolution of natural configuration can result in creep in the composite body. The complete evolution of configuration that happens with composite also happen with individual voxel of the composite. At any time the natural configuration of composite can be different to the natural configuration of the voxel. This difference in motion is called the apparent strain in the composite (Rajagopal & Wineman, 2004). At any voxel in the microstructure, for infinitesimal linearized strain, strain tensor can be approximated as the sum of mechanical strain and the apparent strain (Li et al., 2016).

$$\varepsilon = \varepsilon_{apparent} + \varepsilon_{mechanical} \tag{3}$$

where $\varepsilon_{apparent}$ is the strain associated with the process of dissolution or precipitation changes at the voxel while $\varepsilon_{mechanical}$ is the strain at the voxel associated with the stress field at that voxel. Hence u_{rp} can be written as

$$u_{rp} = U_{rp} + \delta_{rp} + \delta_{rp}^{apparent} \tag{4}$$

where, U_{rp} is the displacement vector determined by the surrounding voxels, δ_{rp} is correction vector which accounts for the boundary conditions and $\delta_{rp}^{apparent}$ is the correction vector which accounts for the apparent strain as a result of phase change due to dissolution and precipitation processes. Clubbing the two correction vectors, $\delta_{rp}^{combined} = \delta_{rp} + \delta_{rp}^{apparent}$ and substituting in the Eq. (2)

$$En = \frac{1}{2}\left[u_{rp}^T D_{rp,sq} u_{sq} + 2\delta_{rp}^{combined} D_{rp,sq} u_{sq} + \delta_{rp}^{combined} D_{rp,sq} \delta_{sq}^{combined}\right] \tag{5}$$

The above equation can be expressed as

$$En = \frac{1}{2} uAu + bu + C \tag{6}$$

where A is the Hessian matrix composed of the stiffness matrices for every voxel/element, b is a constant vector and C is a constant that can be determined by the applied strain and the boundary conditions, and u is a vector of all the displacements. Since Simpson's integration rule can give us exact solution till quadratic order, the exact displacement solution is derived using Simpson's rule such that

$$\frac{\partial En}{\partial u} = Au + b = 0 \tag{7}$$

These calculations to obtain the homogenized elastic properties are done using a previously developed code by National Institute of Standards and Technology (Garboczi, 1998). Since this computational scheme is strain controlled, the microstructure is subjected to constant strain. To predict the time evolving creep strain due to constant external stress, Boltzmann's superposition principle was used (Christensen, 2012; Wineman & Rajagopal, 2000). First a constant strain was applied to the composite at every time step to obtain averaged hydrostatic stress in the composite. Due to dissolution and precipitation process either the stress may relax (due to dissolution) or increase (due to precipitation). If there is both dissolution and precipitation, the dominant process will decide stress relaxation or its increase. If dissolution is the dominating process, in order to keep the stress constant at every loading age, an additional strain must be applied to maintain the constant stress as a function of time. Boltzmann's superposition principle is applied to obtain this applied additional strain using the equations below

$$\text{if i=1, } \varepsilon(t_i) = \frac{-\sigma_0}{3K_{t_i}(t_i)};$$

$$\text{if i}\neq\text{1, } \varepsilon(t_i) = \frac{-\sigma_0 - \sum_{k=1}^{i-1}[\varepsilon(t_k)K_{t_k}(t_i)]}{3K_{t_i}(t_i)}, \tag{8}$$

where, σ_0 is the maintained constant averaged hydrostatic stress, $\varepsilon(t_i)$ is the additional linear strain to be applied to reach the required constant stress, and $K_{t_k}(t_i)$ is the apparent VE/VP bulk modulus of the composite at time t_i when loaded at the age t_k. The total strain, sum of elastic strain and creep strain of the composite as a function of time can be obtained using the following equation

$$\varepsilon_{total}(t_i) = \sum_{k=1}^{i} \varepsilon(t_k); \tag{9}$$

where $\varepsilon_{total}(t_i)$ is the resultant strain of the composite at any time t_i.

2.2. *Implementation on Eagle ford shale*

To illustrate the implementation and applicability of the model, creep deformation was calculated for Eagle Ford shale. The major constituent mineral of this rock is calcite with a mass percentage of 94.4%. It has 3.6% of quartz, 1.1% of kaolinite, 0.9 % of Orthoclase and organic content of 0.37% by mass(Prakash et al., 2019). The porosity of this eagle ford shale was found out to be 5.2%. This sample was selected because of the availability of dissolution and precipitation experimental data for this sample. Also this sample is relatively homogeneous in nature because major proportion of the sample is calcite. This simplifies the analysis and understanding of the results. The computation is done to account for the effect of dissolution and precipitation processes in the shale composite. This dissolution and precipitation process occur when the shale is subjected to supercritical CO_2 and brine at high pressure and temperature conditions (Prakash et al., 2021). This process was simulated in a batch type dissolution reactor in lab, on shale samples of roughly an average dimension of 5 mm. Shale samples were first immersed in a synthetic brine (1M NaCl). Then the samples were pressurized to 1800 psi at a temperature of 100 °C. Two separate reactions were performed with durations of 14 and 28 days (Prakash et al., 2022).

2.3. *Microstructure model*

The microstructure information of the shale is obtained by micro-CT imaging on an unreacted shale sample. Phoenix Nanotom micro-CT scanner was used for performing the micro-CT scans and generate grayscale image slices with a resolution or voxel size of 5 microns. The next step was to assign the different mineral phases to each voxel. The grayscale intensity of each voxel is a function of the atomic number, density and energy source of X-ray which corresponds to a particular mineral phase in the sample. The lower intensity voxels corresponds to lighter minerals and pore spaces while the brighter ones corresponds to denser minerals. Using the intensity histograms and the mineral composition of shale, an informed segmentation was performed using Avizo software (Prakash et al., 2022). This technique is applied to the grayscale images to obtain a 3D microstructure with 4 different phases i.e. calcite-rich, clay/quartz-rich, pyrite-rich and pores. Since the X-ray attenuation coefficient of clay and quartz are very similar, the intensities associated with both the minerals are expected to be very similar. Also the volumetric proportion of clay in the sample is less than 1%, therefore both these phases were combined in the segmentation.

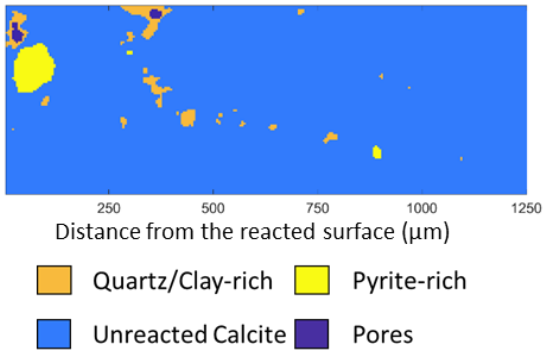

Fig. 1. One of the cross-section of the microstructure of unreacted Eagle Ford shale, showing different.

To reduce the computation cost, a small portion of the microstructure is selected for the analysis. The input microstructure selected for the model is cuboid with 250

x 100 x 40 = 10^6 voxels. Figure 1 shows one of the cross-sections of the microstructure volume. Different colors show different phases of the sample.

Simulations were carried out on Eagle Ford shale with time evolving microstructure as a result of dissolution and precipitation reactions. These reactions were a result of CO_2-rich brine-rock interaction at high temperature and pressure conditions. Nano-indentation and micro-CT analysis were used to study the dissolution and precipitation processes in Eagle Ford shale (Prakash et al., 2019).

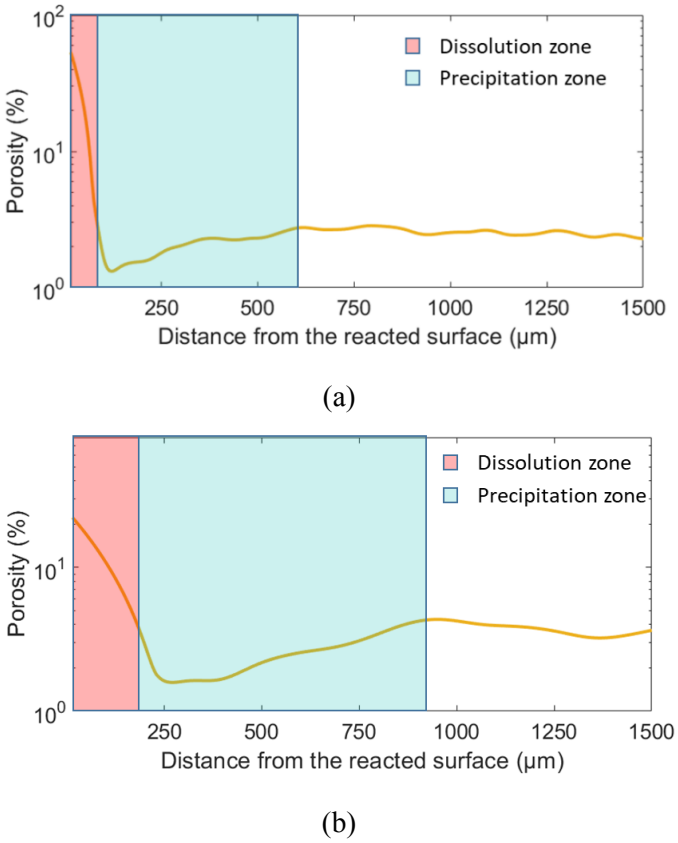

Fig. 2. Variation of porosity versus distance from the exposed surface obtained from micro-CT imaging for eagle ford sample. (a) 14 days reaction (b) 28 days reaction.

Micro-CT analysis was performed on the 14 days and 28 days reacted sample. Change in porosity values were plotted against the distance from the reacted surface (Figure 2). For 14 days reacted sample, the trend shows dissolution (increased porosity) at the exposed surface until a depth of 80 μm. The trend also shows precipitation (decreased porosity) after the dissolution depth, from 80 μm till a depth of 600 μm. After this precipitation depth, constant porosity was observed which indicates no reaction in the sample. Hence the total reaction depth is 600 μm for 14 days reacted sample. Similar dissolution and precipitation pattern was also observed for 28 days reacted sample. In comparison to 14 days reactions, 28 days reacted sample show higher dissolution depth of 150 μm. Precipitation depth is also higher and is seen from 150 μm till a depth of 900 μm. So the total reaction depth is 900 μm for a 28 days reacted sample. The reaction depth is a function of time and seems to follow the Fick's law (Fick, 1855) relationship

$$D(t_i) = k\sqrt{t_i} \tag{10}$$

where, $D(t_i)$ is the reaction depth at any time t_i and k is a constant of proportionality. Assuming this relationship, depth of reaction is calculated for subsequent time steps (42 days and 56 days). Figure 3 shows the increase in reaction depth as the duration of reaction increases.

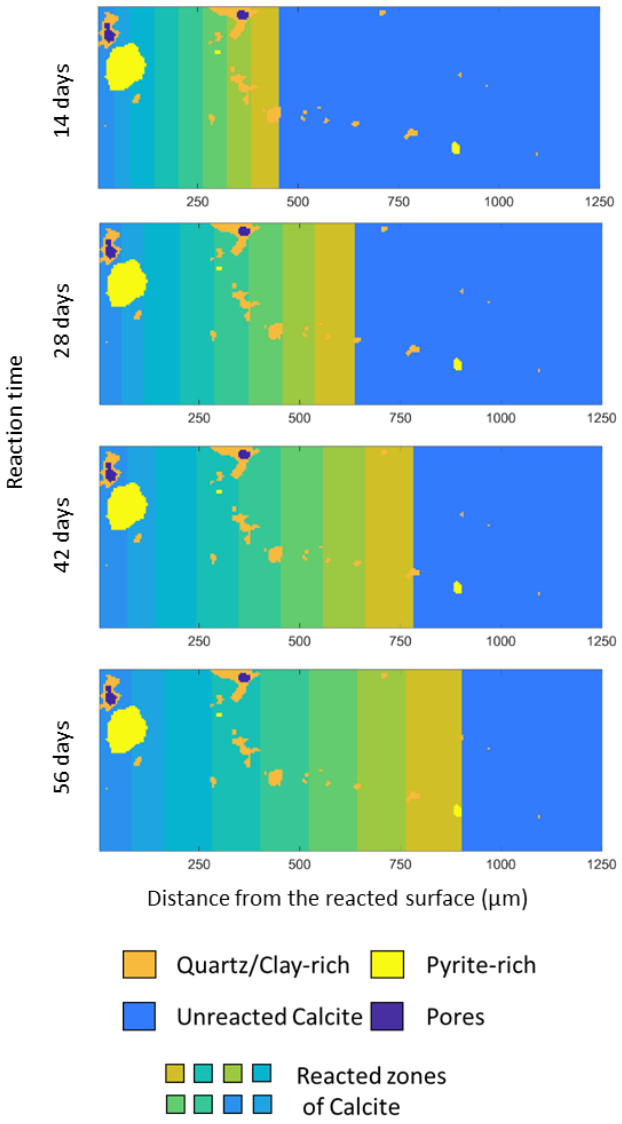

Fig. 3. One of the cross-section of the microstructure of Eagle Ford shale, showing different constituent phases for reacted sample. Microstructure shows time evolving dissolution and precipitation zones at different loading ages (14, 28, 42, 56 days).

Grid indentation analysis (approx. 600 indentation points) was performed on a cross-section of the sample reacted for 14 days, to obtain the variation of modulus as a function of reaction depth (figure 3). A low value of

modulus was found close to the exposed surface. These low values are consistent with the observed high porosity zone from micro-CT analysis. This indicates the formation of dissolution zone where the sample is weakened by dissolution of calcium carbonate. After this region, a high modulus zone was observed. This increase in modulus is due to the precipitation of calcium carbonate inside the pores. Micro-CT result confirms this by showing decreased porosity in that zone.

3. RESULTS

The finite element simulation is done at 5 time steps (0, 14, 28, 42, and 56 days) as shown in figure 1 and 3. At every time step changes in microstructure is done by changing the mechanical property of calcite-rich zone is the sample according to experimental results presented in figure 4. Modulus of pyrite-rich and clay/quartz rich zones are assumed to be constant at every time step. This is a good assumption attributing to the small compositional volumes of these minerals. Also, this assumption simplifies the microstructure. The calcite rich zone in reacted portion of the sample is divided into 8 zones of different mechanical properties. These mechanical properties are obtained from the indentation data (fig 4). For 14 days reaction the modulus in a particular zone is calculated as the average modulus in that zone. Once the modulus is assigned to the zone, it is kept same for the subsequent time steps, only the distance from the exposed surface and thickness of these zones change with time. The thickness of these zones increase according to the equation 10, which is derived from the micro-CT analysis (figure 2).

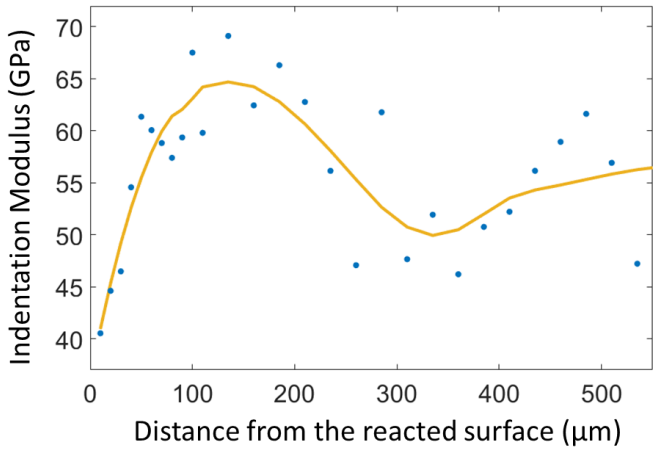

Fig. 4. Variation of Indentation modulus of carbonate phase across the depth of reaction for Eagle Ford shale.(Prakash et al., 2022)

At the first time step (t_i =0), a hydrostatic strain of 140 µstrain was applied such that the averaged hydrostatic stress is same as the experimental pressure condition, i.e. 1800 psi. At the next time steps the same strain was applied to the updated microstructure. A stress relaxation was observed at every time step, indicating the dominance of dissolution reaction. Using the Boltzmann's equation, the creep strain at all time steps is calculated. Fig. 5 shows the predicted creep of the Eagle Ford shale in hydrostatic strain while excluding the instantaneous elastic deformation due to loading. This creep is the total creep at the end of that loading age. In Fig. 5 it can be seen that the shale sample continues to creep under constant pressure as a result of dissolution or reduction in mechanical properties of the load bearing phases. Fig. 6 shows the decrease in viscoelastic bulk modulus of the Eagle Ford shale with the increase in loading age. Once the creep strain is calculated at each time step, this creep strain is utilized to plot the creep strain field in the sample. Fig. 7 shows the map of volumetric creep strain after 14 days of loading. High values of creep strain can be seen in the dissolution zones and softer zones of clay/quartz-rich zones. Creep strains are lower in hard pyrite zone (circular blue region).

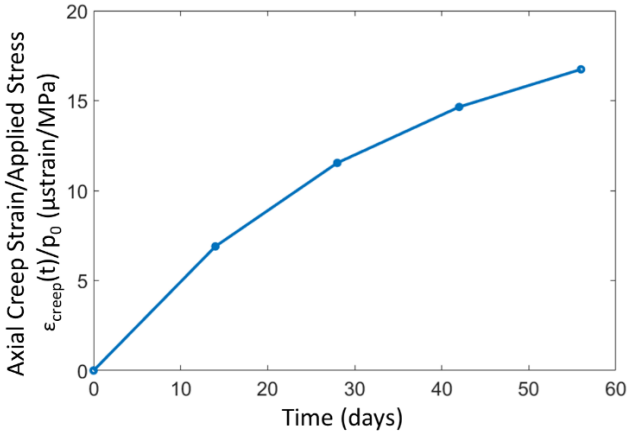

Fig. 5. Axial creep strain of Eagle Ford sample at different loading ages.

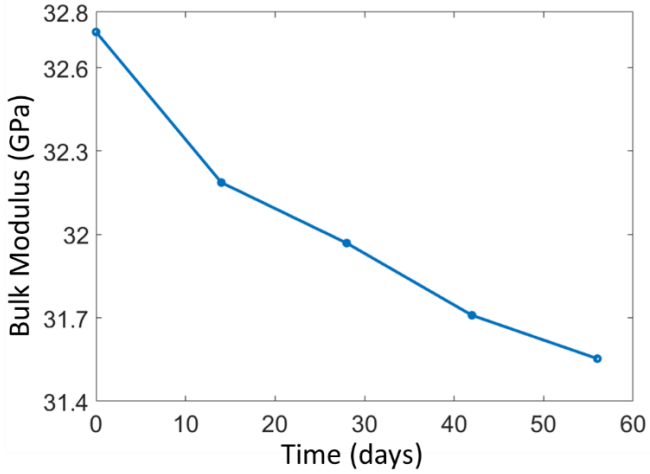

Fig. 6. Viscoelastic Bulk Modulus of Eagle Ford shale at different loading ages.

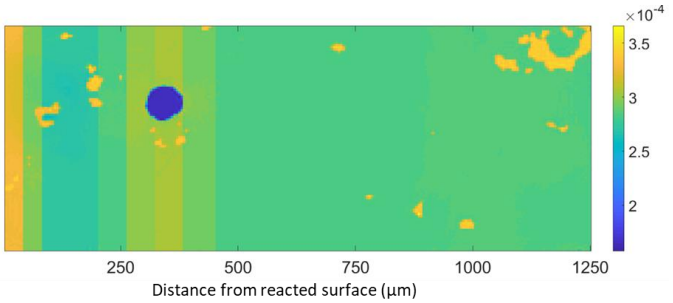

Fig. 7. Volumetric creep strain field at one of the cross-section of the microstructure after 14 days of loading.

4. CONCLUSIONS

A computational scheme utilizing the mechanical data from nano-indentation test and microstructural evolution data from micro-CT imaging was successfully implemented to calculate the time dependent creep strain. Time dependent microstructural model and a finite element model were coupled to establish the computational scheme. The approach was applied to Eagle Ford shale sample to predict the viscoelastic behavior when it is exposed to CO_2-rich brine at high temperature and pressure condition. The total creep strain in the composite was a result of dissolution and precipitation process in the sample. Variation of viscoelastic bulk modulus of the sample with time shows a decline trend. Creep strain field is computed which shows the creep behavior of different zones of reaction in the sample. Prediction models shows high creep strain in the dissolution zone at the exposed surface which can play an important role during hydraulic fracturing processes.

This study has been implemented on a simple microstructure where the microstructural changes come mainly from dissolution and precipitation of calcite. Hence, further studies on more heterogeneous samples constituting other reactive minerals, remain necessary to investigate the contribution of creep strains due to microstructural evolution of those minerals.

REFERENCES

1. Christensen, R. (2012). *Theory of Viscoelasticity: An Introduction*. Elsevier Science.
2. Du, J., Hu, L., Meegoda, J. N., & Zhang, G. (2018). Shale softening: Observations, phenomenological behavior, and mechanisms. *Applied Clay Science*, *161*(May), 290–300. https://doi.org/10.1016/j.clay.2018.04.033
3. Fick, A. (1855). Ueber Dqfusion; *Annalen Der Physik*, *94*, 59–86.
4. Garboczi, E. (1998). Finite element and finite difference programs for computing the linear electric and elastic properties of digital images of random materials. Rep 6269. *NIST Interagency/Internal Report (NISTIR) - 6269*.
5. Haecker, C. J., Garboczi, E. J., Bullard, J. W., Bohn, R. B., Sun, Z., Shah, S. P., & Voigt, T. (2005). Modeling the linear elastic properties of Portland cement paste. *Cement and Concrete Research*, *35*(10), 1948–1960. https://doi.org/10.1016/j.cemconres.2005.05.001
6. Li, X., Rahman, S., & Grasley, Z. C. (2016). Computationally implemented modeling of creep of composite materials caused by phase dissolution. *Computational Materials Science*, *125*, 61–71. https://doi.org/10.1016/j.commatsci.2016.08.030
7. Prakash, R., Christian, P., Nguene, K., Benoit, D., & Henkel, K. (2021). Assessment of local phase to mechanical response link: application to the chemo-mechanical identification of rock phases subjected to reactive environments. *Journal of Natural Gas Science and Engineering*, 103857. https://doi.org/10.1016/j.jngse.2021.103857
8. Prakash, R., Christian, P., Noshadravan, A., & Abedi, S. (2022). Chemical reactions of carbonate-rich shale rocks with aqueous CO2 and their impacts on shale's local microstructural and mechanical properties. under review.
9. Prakash, R., Kana Nguene, P., Seers, T. D., Noshadravan, A., & Abedi, S. (2019). Chemo-mechanical investigation of CO 2 -fluid-rock interaction in CO 2 storage and CO 2 -EOR processes in unconventional reservoirs. *American Rock Mechanics Association*.
10. Rajagopal, K. R., & Wineman, A. S. (2004). A note on viscoelastic materials that can age. *International Journal of Non-Linear Mechanics*, *39*(10), 1547–1554. https://doi.org/10.1016/j.ijnonlinmec.2003.09.001
11. Rybacki, E., Meier, T., & Dresen, G. (2016). What controls the mechanical properties of shale rocks? - Part II: Brittleness. *Journal of Petroleum Science and Engineering*, *144*, 39–58. https://doi.org/10.1016/j.petrol.2016.02.022
12. Sharma, P., Prakash, R., & Abedi, S. (2019). Effect of temperature on nano- and microscale creep properties of organic-rich shales. *Journal of Petroleum Science and Engineering*, *175*. https://doi.org/10.1016/j.petrol.2018.12.039
13. Sone, H., & Zoback, M. D. (2010). Strength, creep and frictional properties of gas shale reservoir rocks. *44th US Rock Mechanics Symposium - 5th US/Canada Rock Mechanics Symposium*.
14. Sone, H., & Zoback, M. D. (2013). Mechanical properties of shale-gas reservoir rocks - Part 2: Ductile creep, brittle strength, and their relation to the elastic modulus. *Geophysics*, *78*(5). https://doi.org/10.1190/GEO2013-0051.1
15. Sone, H., & Zoback, M. D. (2014). Time-dependent deformation of shale gas reservoir rocks and its long-term effect on the in situ state of stress. *International Journal of Rock Mechanics and Mining Sciences*, *69*, 120–132. https://doi.org/10.1016/j.ijrmms.2014.04.002
16. Wineman, A. S., & Rajagopal, K. R. (2000). *Mechanical Response of Polymers: An Introduction*. Cambridge University Press.